IJEP 43 (6) : 483-492 (2023) (ISSN : 0253-7141)

An Ecological Problem of Heavy Metal Removal by using Green Synthesized Magnetically Recovery Fe_3O_4@ZnO Nanocomposites

C. Mohankumar[1], S. Sathian[1]*, P. Akilamudhan[2] and A. Murugesan[3]

1. Annamalai University, Department of Chemical Engineering, Chidambaram, Tamil Nadu - 608 002, India
2. Erode Sengunthar Engineering College (Autonomous), Department of Chemical Engineering, Erode, Tamil Nadu - 637 205, India
3. Nandha Engineering College, Department of Chemical Engineering, Erode, Tamil Nadu - 638 052, India

*Corresponding author, Email: sathee.selvakumar@gmail.com; petromohankumar@gmail.com

The ability to reuse adsorbent was critical for making the sewage treatment system both premium and environmentally beneficial. Toxic metal ions [Pb (II), Cr (II) and Cd (II)] were removed from effluent discharge using Fe_3O_4/ZnO nanoparticles as sorbent materials. Chemical affinity, zero potentials, XRD, FTIR and TEM were used to explore the structural and interface adsorption process of Fe_3O_4/ZnO composite in this study. Experiments on absorption, desorption and recycling were performed. The findings demonstrate that perhaps the toxic metals substituted for H in the Fe–O–H structure and formed the Zn–O–Me structure, implying that metal elimination was accomplished through ion exchange. Cd (II), Pb (II) and Cr (IV) had 99.81%, 99.76%, 98.1% and 83.25%, accordingly, adsorptive degradation efficiency. The Langmuir model was shown to be the best fit for describing the absorption on the surface of Fe_3O_4/ZnO nanoparticles based on the stability data processing. The kinetic parameters of toxic metal ions on the surface of Fe_3O_4/ZnO composites were relatively similar to the pseudo-second-order concept, according to the kinetics investigations. The trials proved that reprocessing the Fe_3O_4/ZnO sorbent extracted from water by a magnetic material was a viable option for removing pollutants in an environmentally acceptable and effective manner.

KEYWORDS

Heavy metals, Fe_3O_4/ZnO, Adsorption, Magnetite, Langmuir isotherm

1. INTRODUCTION

Presently, ecological regulation is a serious problem in the world. Water contamination is probably of the most concerning aspects of society. Extensive variety of emissions, such as toxic metals, colours and fertilizers, reach various waterways and become important contributors to groundwater contamination [1]. Toxic metals are particularly dangerous because of their great water fluidity and greater accessibility to live bodies across the food system, resulting in a variety of health complications [2]. Lead (Pb), chromium (Cr) and cadmium (Cd) are toxic substances that are a major contaminants and are extensively distributed [3]. Consuming contaminated watercourses via a range of sources, including electrolysis, mining, metal polishing and lead, chromium and cadmium casting [4]. Various approaches for removing contaminants have been intensively examined in the literature. To eliminate toxic metal ions from polluted water, various methods, such as co-precipitation, electrochemical methods, membrane processes and absorption have been developed [5]. Because of its high removal effectiveness, dependability, affordability and lack of toxic byproducts, adsorption was an appealing strategy in polluted water remediation among these approaches [6]. Several methods for developing less expensive and more powerful material adsorbents have previously been explored [7].

Minerals have received more attention in the last decade for toxic substances cleanup treatments due to their excellent sorption capacities [8,9]. The nanostructured material, especially, offers extremely large surface areas, resulting in high capacity and the ability to improve contaminant's adhesion with the interface [10,11]. As a result, Fe_3O_4/ZnO was chosen as a component in the preparation of overlayed sorbent materials for the elimination of heavy metals [12,13]. Regrettably, such materials still had difficulty with removal from polluted water, as they preferred to form

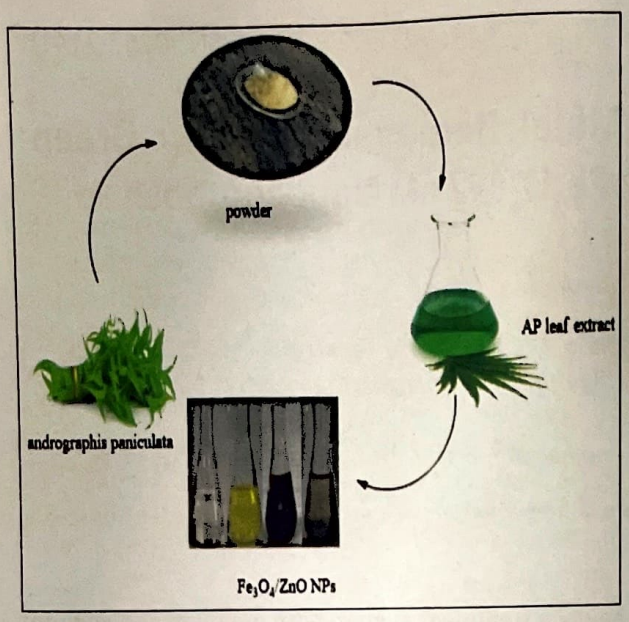

Figure 1. *Formation of Fe_3O_4@ZnO nanoparticles using green synthesis route*

ultra-fine granules in aqueous phase, resulting in prior to actual. As a result, the creation of novel nano sorbents with easy separation properties and reuse potential has piqued our attention. Due to their strong magnetic permeability, iron oxides, like magnetite (Fe_3O_4) and hematite (Fe_2O_3) have been widely used in construction. The addition of Fe_3O_4/ZnO resulted in not only excellent elimination of heavy metals from aqueous solution but also recuperation due to its magnetic properties. Interface functionalization was discovered to be responsible for absorption. There was a limitation in understanding exterior structure-sensitive absorption and the operation of absorption. It's still unclear how the variable impact heavy metals' adhesion and the adsorbent's effectiveness in multiple reuse.

Toxic metals, such as Pb (II), Cr (IV) and Cd (II) were removed from industrial effluents using Fe_3O_4/ZnO composites as cycling sorbents in this analysis. Structural and optical properties and performance of Fe_3O_4/ZnO composites were investigated. In order to eliminate pollutants from wastewater water, the permeate parameters were evaluated. The composite materials' molecular affinity and cumulative capability were considered to be effective to ascertain heavy metals in wastewater. Fe_3O_4/ZnO composites' surface adsorption behaviour and kinetics were examined. Heavy metal adsorption and desorption, as well as recycling, were investigated. The metal uptake methods of Fe_3O_4/ZnO nanocomposite sorbent have been explored. Throughout this content analysis, core-shell Fe_3O_4/ZnO nanoparticles have been synthesized and used to accumulate commercial effluents, such as lead, chromium and cadmium ions. The influence of interaction period, aqueous phase pH, catalyst dosage, initial effluent composition and heating rate on adsorption were evaluated. Following that, the kinetic models, stability [illegible] transfer analyses have been examined.

2. MATERIAL AND METHOD

2.1 Green synthesis of Fe_3O_4 nanoparticles

At 80°C, 10 g of crisped *Andrographis paniculata* leaf extract was injected into demineralized water. The water extract was used to make Fe_3O_4 magnetic nanoparticles after the combination had been diffused for 2 hr. $FeCl_3$ (2 mmol) and $FeCl_2$ (1 mmol) were added to a 100 mL *Andrographis paniculata* leaf water extract in a two-necked round-bottomed flask (250 mL). Under an inert atmosphere and at room temperature, a solution of NH_4OH was gently added to the mixture. External magnetic field was used to develop and detach the pure black crude product from the precursor resolution, which was then vacuumed and washed repeatedly before being oxidized in an oven at 80°C for 24 hr [14].

2.2 Design and fabrication of Fe_3O_4/ZnO nanocomposites

To design and build of Fe_3O_4/ZnO nanocomposite in demineralized water, 1.5 g of $Zn(OAC)_2$, 1.5 g of $FeCl_2.4H_2O$ and 1.5 g of $FeCl_3.5H_2O$ were solubilized (10 mL). In a round-bottomed flask at 85°C for 8 hr *Andrographis paniculata* leaf (APL) extract (30 mL) was gradually added to the reaction mixture. To eliminate undesirable plant-based matter, the mixture was cooled to room temperature, sonicated for 10 min, resuspended at 7000 rpm for around 10 min and afterwards purified. Prefilter was used to accumulate the crude product followed by multiples rinses with deionized water and ethanol (96%). The specimens were then warmed for 1 hr at 50°C. The fabrication of Fe_3O_4/ZnO nanocomposites was dehydrated in the air for 24 hr at room temperature (Figure 1) [15].

2.3 Investigation of removal of heavy metals

Heavy metals [Pb (II), Cd (II), Cr (IV)] were present in commercial effluent at concentrations of 10 mg/L. For removal of toxic metals from industrial effluents, a magnetic Fe_3O_4/ZnO composite was used as an adsorbent. The adsorptive Fe_3O_4/ZnO composite was implanted in contaminated water and agitated for 24 hr on a spinning tank (20 rpm). Investigations of heavy metal removal were performed at pH levels ranging from 2-12

Table 1. *Different parameters of various isotherm models*

Heavy metals	Langmuir isotherm			Freundlich isotherm		
	q_m	K	R^2	K'	n	R^2
Cd^{2+}	568.3	7.92	0.9920	152.3	2.673	0.798
Cr^{4+}	602.6	0.90	0.978	160.9	2.920	0.934
Pb^{2+}	670.2	3.26	0.992	178.26	2.820	0.936

Table 2. *Kinetic adsorption parameters*

Heavy metals	Pseudo first order		Pseudo second order	
	K_L	R^2	K	R^2
Cd^{2+}	0.0042	0.9599	0.0386	0.998
Cr^{4+}	0.0038	0.9402	0.0142	0.999
Pb^{2+}	0.0061	0.7382	0.0048	0.994

and temperatures tend to range from 30-60°C. The adsorptive composites were then gathered from the solution using a NdFeB magnet. After removal of toxic substances, the contaminated water was analyzed using inductively coupled plasma emission spectra spectrophotometry (ICP). Every batch process was repeated three times, as well as the comparable discrepancy was noticed to be less than 2%, with the final results being the sample mean. The expulsion level was predicted using the capacity of retrieval of heavy metal ions in solution prior to actually and during the adsorption and the expression as follows :

$$q_e = (C_o - C_e)/(C_o) \quad \ldots (1)$$

Where q_e (%) is removal degree, C_o and C_e (mg/L) are the initial and final metals concentrations in the solution, respectively. For the adsorptive investigation, Fe_3O_4/ZnO and toxic metals were immersed in the 0.1 M HCl solution and the resulting mixture was shaken vigorously in a shaking incubator at 30°C for 0.5 hr. The composite feedstock was then gathered using a NdFeB magnet and metal ion doses in the solution were measured. Upon rinsing, Fe_3O_4/ZnO nano-composite has been used in the succeeding adsorbent cycle. The amount of ions desorption per unit volume of adsorptive used was calculated from the respective approximation.

$$q_{de} = (CV_0/m_0) \times 100 \quad \ldots(2)$$

Where q_{de} was the desorption degree (%), C was the metal ion accumulations in the desorption solution (mg/L), V_0 was the volume of the desorption solution (L) and m_0 was the quantity of toxic metal ions in solution before desorption (mg).

2.4 Adsorption isotherm

The Freundlich and Langmuir models have already been employed to investigate adsorption characteristics [16]. The Langmuir isotherm model was determined by calculating the adsorption performance and offered the adsorbent's fairly homogeneous acceleration. This isotherm also implied monolayer adsorption. Equation 3 denotes the simple regression analysis of the Langmuir model. The Freundlich arithmetic model describes both monolayer and multilayer adsorbents. Freundlich isotherm model was traditionally used to identify strong adsorption ability. Equation 4 affirms the linear function of the Freundlich model.

$$C_e/q_e = 1/kq_m + C_e/q_m \quad \ldots(3)$$

$$\log q_e = \log k' + 1/n \log C_e \quad \ldots(4)$$

Where C_e is the equilibrium concentration of heavy metal ions (mol/L) and q_e is the corresponding value of volume of heavy metal ions adsorption at equilibrium (mg/g), k is the Langmuir isotherm constant and q_m is the extreme monolayer coverage capacity (mg/g), n is associated to adsorption capacity and k' is the Freundlich isotherm constant (mg/g) (L/mg). Constraints of many isotherm models are specified in table 1.

2.5 Adsorption kinetics

The rate of adsorbed heavy metal ions on the surface of the sorbent was determined by studying the adsorption kinetics. The most popular kinetic models for modelling the kinetic rates are pseudo-first order and pseudo second order models [17]. The amount of heavy metals adsorbed on the surface of the sorbent at various time intervals was also determined using these models. These models' equations can be written as given in equations 5 and 6.

$$\ln (q_e - q_t) = \ln q_e - k_L t \quad \ldots(5)$$

$$t/q_t = 1/kq^2_e + 1/q_e \times t \quad \ldots(6)$$

Where q_e (mg/g) is amount of heavy ions adsorption at equilibrium condition, q_t (mg/g) is heavy ions adsorption amount at time t, K_L and K represents the rate constants of pseudo-first order and second order models, respectively. In the pseudo-first-order model, q_t and t had an exponential relationship, whereas in the pseudo-second-order model, the relationship between t/q_t and t was linear. Table 2 lists adsorption parameters.

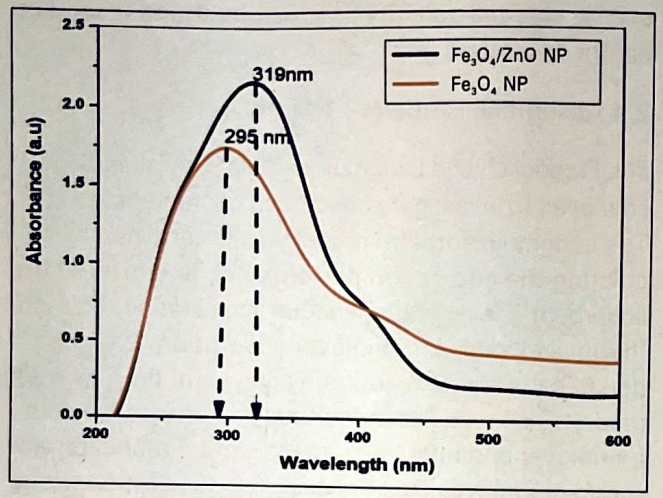

Figure 2. *UV absorption spectra of (a) Fe_3O_4 and (b) Fe_3O_4@ZnO nanoparticles*

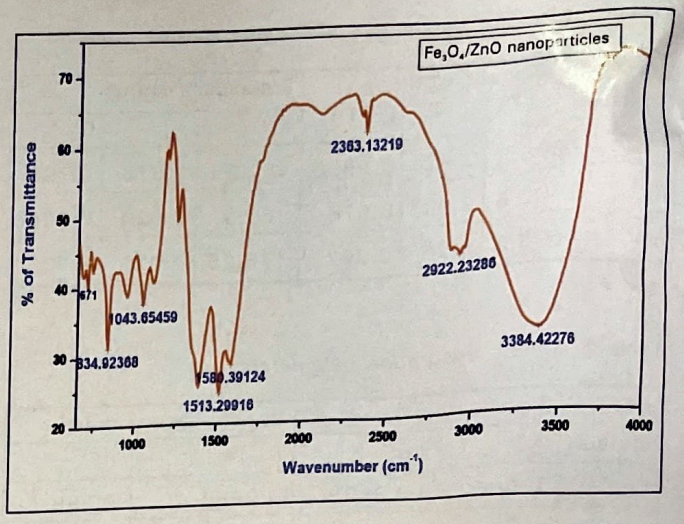

Figure 3. *Representation of functional group in Fe_3O_4@ZnO nanoparticles*

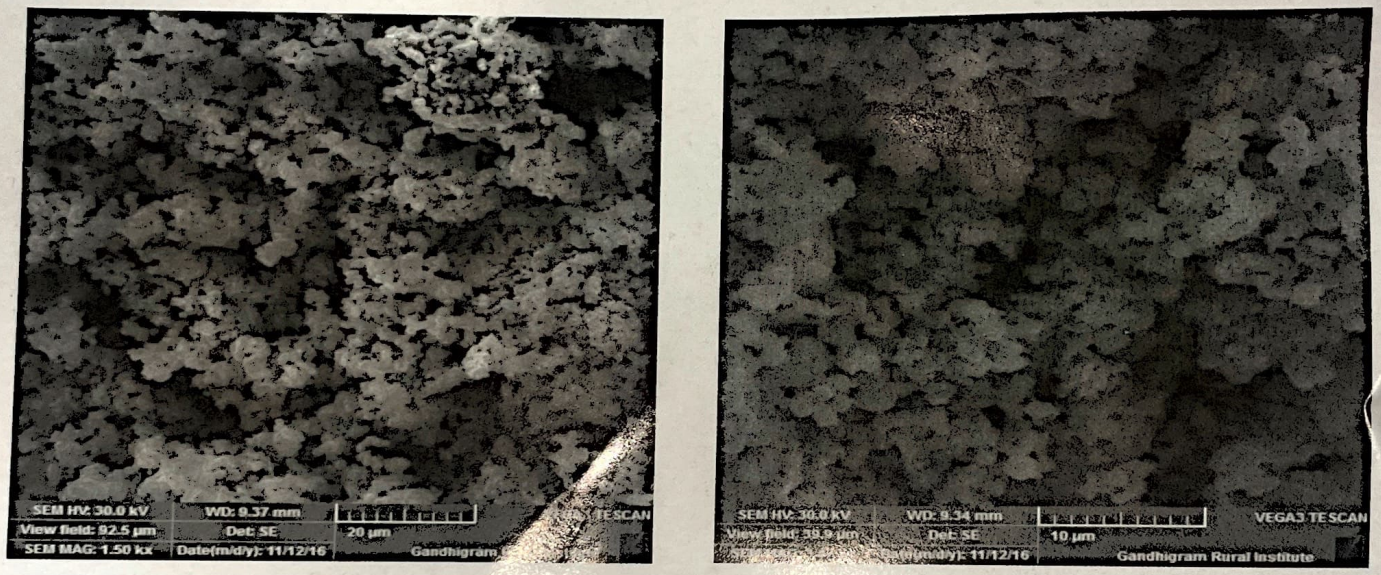

Figure 4. *SEM profile of Fe_3O_4@ZnO nanop*

3. RESULT AND DISCUSSION

3.1 UV absorption spectra analysis

Figure 2 illustrates the UV–visible recogn[illegible] peaks of Fe_3O_4/ZnO nanocomposites. Once *Andrographis paniculata* leaf extract was infused with $Zn(OAC)_2$, $FeCl_2.4H_2O$ and $FeCl_3$. $5H_2O$, the colour change from white to brown was observed, which was credited to the formation of Fe_3O_4/ZnO nanocomposites. The colour variations are accompanied by the fluctuation of localized surface plasmonic resonance (LSR) of Fe_3O_4/ZnO nanocomposites. The broad absorption peaks were found to be near 319 nm, indicating a substantial decrease of $Zn(OAC)_2$ and Fe^{3+}/Fe^{2+} into Fe_3O_4/ZnO nanocomposites [18,19].

3.2 Fourier transforms infrared spectroscopy analysis

Figure 3 depicts FTIR spectrum of ecofriendly synthesized Fe_3O_4/ZnO nanocomposites. The frequency spectrum bands at 3384.4/cm has been caused by O-H stretching. The band around 2363 - 2922/cm is engen[illegible]d by C–H stretching vibrations. The peak inside 1580-1513/cm is induced by C=O stretching. The peaks at 1043/cm coincide with Fe-O-Zn twisting compressive motions. The squeezing variants for the emergence of Fe_3O_4/ZnO nanoparticles are delegated by potent excitation frequency band at 671/cm. As a consequence of FTIR survey, Fe_3O_4/ZnO nanocomposites are preserved from becoming ascertained by the bioactive constituents of *Andrographis paniculata* leaf

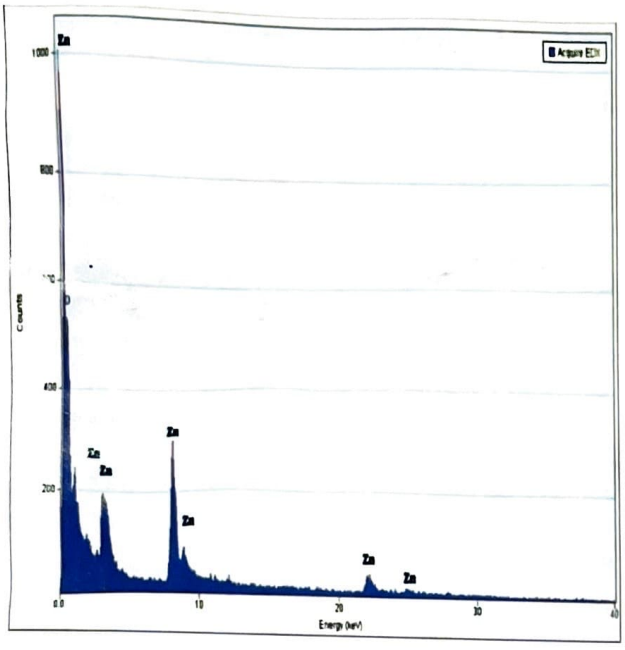

Figure 5. *EDX profile of Fe_3O_4@ZnO nanoparticles*

by stabilizing the exterior of nano-composites during synthesis process [18,19].

3.3 X-ray diffraction analysis

X-ray diffraction (XRD) analysis was used to investigate phase and structural components of Fe_3O_4/ZnO nanocomposites in figure 3. The cubic spinel magnetite component is visible in XRD analysis of Fe_3O_4, with crystallography peaks at 30.20°, 35.59°, 43.22°, 54.04°, 57.25° and 62.87°, corresponding to (220), (311), (400), (422), (511) and (440) planes, respectively. The XRD behaviour of Fe_3O_4/ZnO nanocomposites shows all magnetite defining feature peaks as well as crystallography peaks at 31.76°, 34.42°, 36.08°, 47.53°, 56.76° and 62.80° that can be accessed to (100), (002), (101), (102), (110) and (112) planes of the hexagonal wurtzite phase of ZnO. This indicates that the ZnO shell was successfully formed without any phase transition of Fe_3O_4 nanoparticles [20].

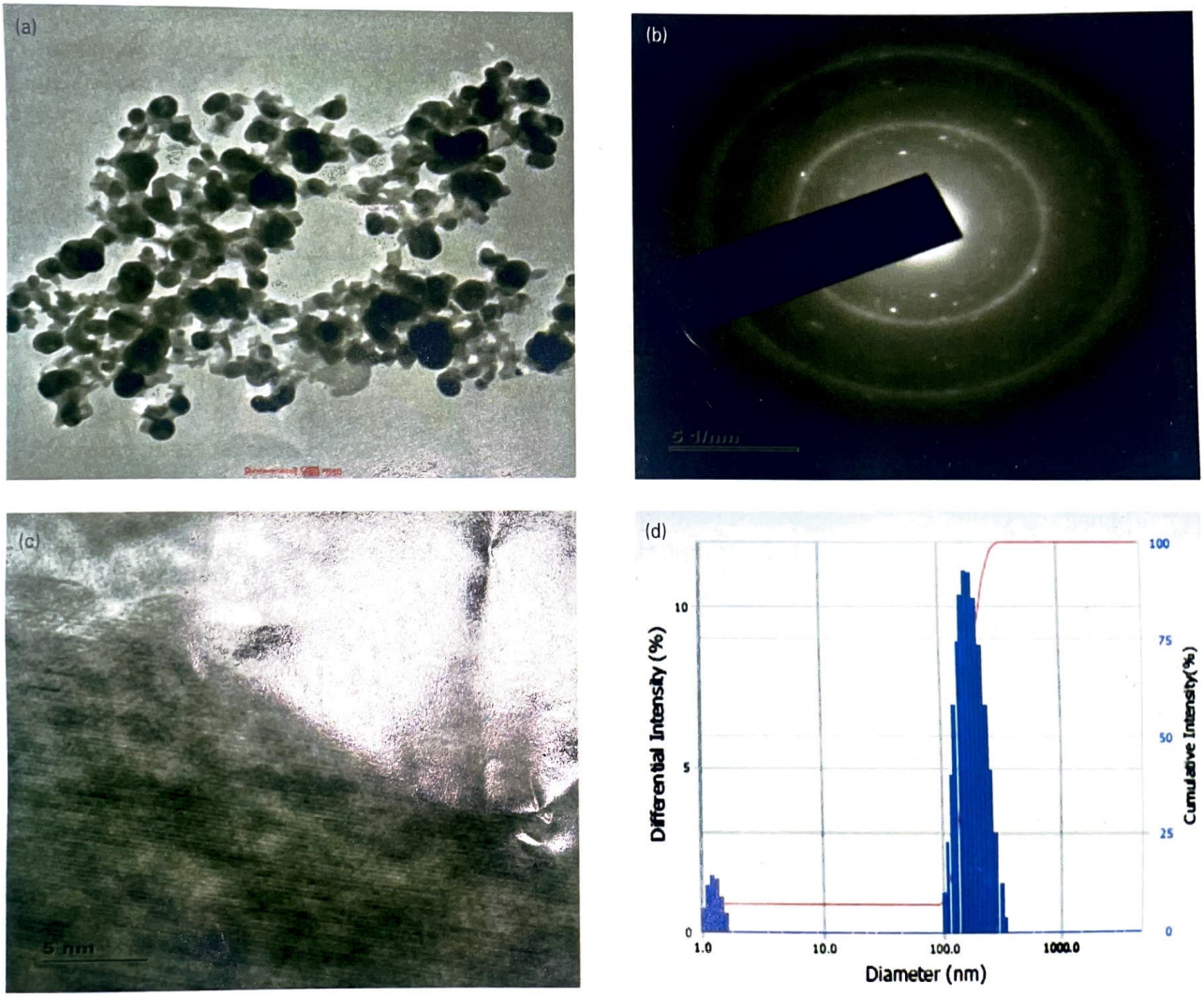

Figure 6. (a) *TEM profile, (b) SAED pattern analysis, (c) HR TEM profile and (d) DLS analysis*

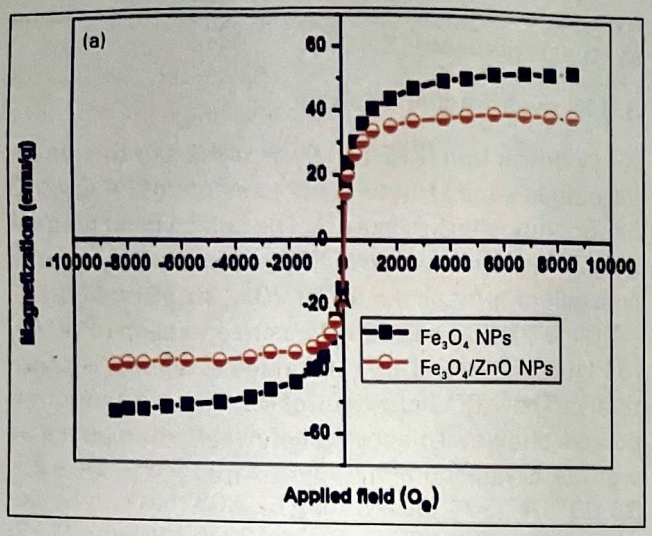

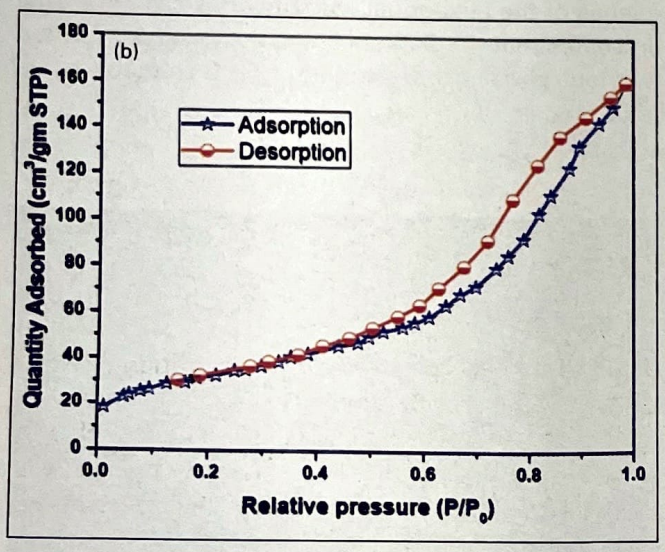

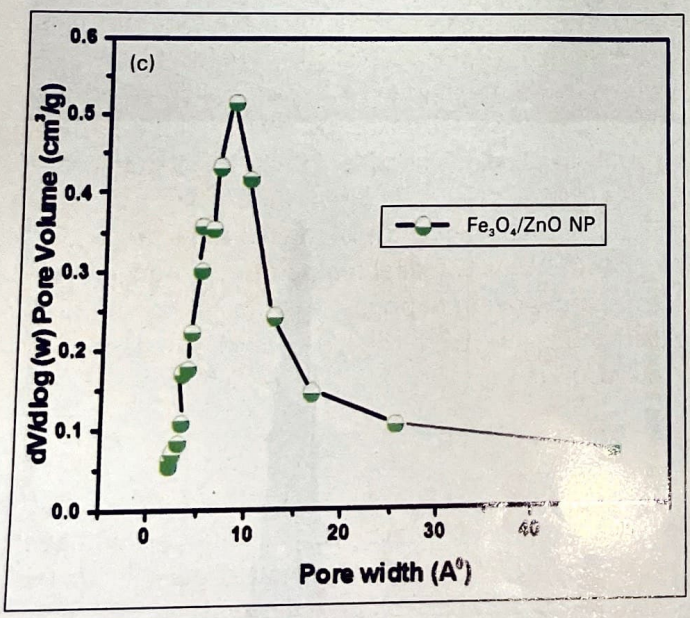

Figure 7. *(a) VSM spectra of Fe_3O_4 and Fe_3O_4/ZnO nanoparticles, (b) BET isotherm graph and (c) pore width of synthesized Fe_3O_4/ZnO nanoparticles*

3.4 SEM/EDX analysis

Scanning electron microscopy (SEM) investigation was used to examine the architecture of Fe_3O_4/ZnO nanoparticles. The outcome of the study shows that the fabricated Fe_3O_4/ZnO particles were globular and consolidated into an anisotropic material with a mean size of 18 nm, as shown in figure 4. The powder particles were found to be somewhat clustered [21]. Figure 5 shows energy dispersive x-ray spectrum of green fabricated Fe_3O_4/ZnO nanoparticle specimens, which confirms the existence of Fe, Zn and O constituents. The absence of an imperfection band in the EDX spectrum proves that the synthesized samples are genuine and also demonstrates homogenous allocation of the individual components.

3.5 TEM/HRTEM analysis

The transmission electron microscopy (TEM) appearance and selected area (electron) diffraction (SAED) profile of Fe_3O_4/ZnO nanocomposites developed using the green approaches are shown in figure 6. The mean particle size in figure 6a was determined to be 11 nm, which was quite close to crystalline phase predicted in XRD pattern using Debye Scherrer's model. Figure 6b shows that reflection bands in SAED illustration correspond to XRD profile, confirming crystallite size and anatase phase of Fe_3O_4/ZnO nanoparticles [22]. The dynamic light scattering (DLS) method was used to identify the particle sizes and average diameter of the synthesized Fe_3O_4/ZnO, as seen in figure 6d. These figures state that overall size and monodispersity index (PDL) of synthesized Fe_3O_4/ZnO using *Andrographis paniculata* leaf extract and derivatives were 295 and 0.31 nm, respectively and 61.44 and 0.42 nm. The calibrated z-average and polydispersity index of the synthesized Fe_3O_4/ZnO nanocomposites show narrow size distribution, correlating with the facts provided either by distributor or ultraviolet - visible analysis [23].

3.6 BET isotherm spectra

The Brunauer-Emmett-Teller (BET) surface area analysis tool was used to determine actual area of produced nanomaterials. Barrett-Joyner-Halenda study also yielded other results, such as pore diameter and average pore. The produced Fe_3O_4/ZnO nanoperticles exhibited excellent surface area of 105 m^2/g, pore size of 50 nm and volume fraction of 0.278 cm^3/g, which will be useful for photocatalytic activity in treatment of contaminated (Pb(II), Cr(IV), Cd (II)) wastewater. Figure 7b shows acquired adsorption-desorption isotherm models of the produced Fe_3O_4/ZnO nanoparticles [24].

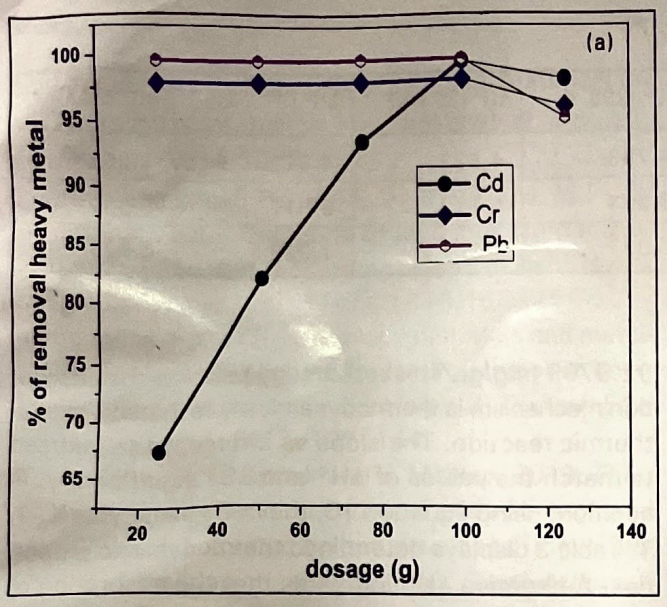

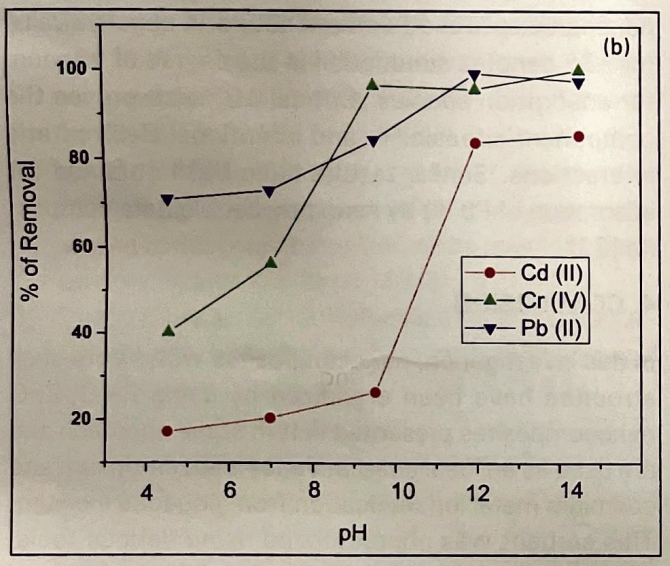

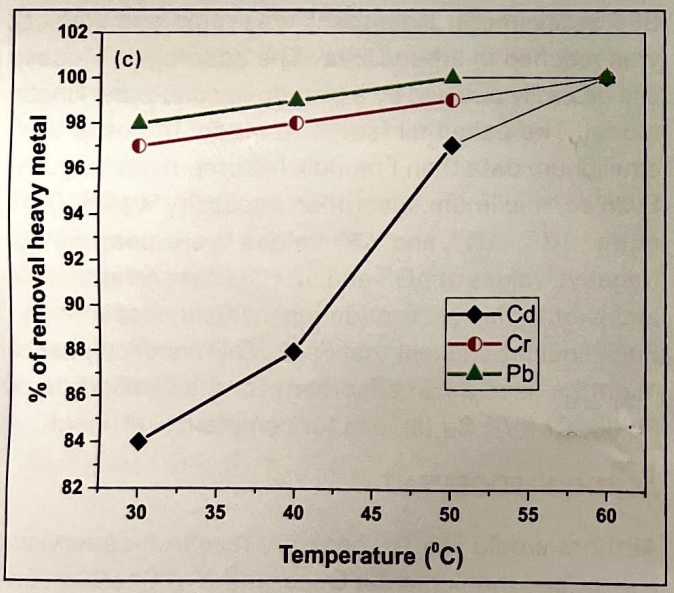

Figure 8. *(a) Effect of adsorbent dosage, (b) temperature and (c) pH on removal of metals from wastewater*

3.7 Magnetic behaviour analysis

According to the field-dependent magnetic properties graphs (Figure 7a), the magnetization interaction of both Fe_3O_4 and Fe_3O_4/ZnO nanoparticles is pricey but nearly sequential at lower energies and while at greater domains, fragments are nearly connected with applied magnetic field and the magnetization strategies saturation. The coercivity and remanent magnetization of Fe_3O_4 nanoparticles were measured to be 15 Oe and 0.3 emu/g, respectively, whereas those Fe_3O_4/ZnO nanoparticles had 7.5 Oe and 0.8 emu/g. The presence of fairly minimal co-ercivity and remanent magnetization indicates that these materials showed superparamagnetic actions at ambient temperature. Besides that, at 5 T, the maximum magnetic moment value of Fe_3O_4@ZnO nanoparticles (31.2 emu/g) was realized to be substantially lower than that of Fe_3O_4 nanoparticles (35.8 emu/g). Magnetic moment has revealed that the ZnO shell in Fe_3O_4/ZnO nanoparticles contributed significantly to a 12% lowering in the magnetic moment value of Fe_3O_4. As a consequence, the excellent magnetic field responsiveness of Fe_3O_4/ZnO is sustained [24].

3.8 Impact of temperature

One of the most crucial factors in absorption process is the effect of temperature. The effect of temperature on the ability of Fe_3O_4 @ ZnO nanoparticles to adsorb in the range of 30-60°C at room temperature is shown in figure 8b. It is evident from figure 8b that a rise in temperature causes a rise in the elimination of Pb (II), Cd (II) and Cr (IV) from aqueous solutions. As seen, adsorption happened quickly and equilibrium was established after 2 hr. Due to great dispersion of nanoparticles, the high exterior surface area and the absence of internal diffusion constraint, this rapid adsorption can be explained [25,26]. Little change in the absorption rate after the first 10 min, which indicates that process would eventually attain equilibrium. Fe_3O_4/ZnO at 50°C was the ideal temperature for adsorption process employing nanocomposites. As a result, all experiments were run at 60°C to assure a perfect equilibrium state.

3.9 Effect of adsorbent dosage

Using different doses of nanoparticles, the impact of adsorbent dosage on adsorption capacity and removal efficiency was studied. According to figure 8a, as the amount of adsorbent is increased from 0.1 to 2 g/L, the removal efficiency of Pb (II), Cd (II) and Cr (IV) increases from 26.97 to 96.08%. More binding sites are available as a result. On the other hand, as adsor-

Table 3. *Thermodynamic parameters for adsorption of Cd^{2+}, Cr^{4+}, Pb^{2+}*

Heavy metals	ΔH° (J/mol)	ΔS° (J/mol/K)	ΔG° (298 K)	ΔG° (303 K)	ΔG° (313 K)	ΔG° (323 K)
Cd^{2+}	-18.936	-49.274	-4.793	-4.632	-4.321	-3.261
Cr^{4+}	-20.638	-54.283	-6.234	-6.123	-6.012	-5.234
Pb^{2+}	-24.726	-58.324	-7.322	-7.221	-7.023	-6.023

bent dosage is increased within the same range, adsorption capacity reduces from 269.7 to 48.04 mg/g. The cause of this phenomenon is that, with increased adsorbent dosage, the number of existing ions was insufficient to completely saturate the active sites. Actually, the ratio of metal to binding sites determines adsorption capability.

3.10 Effect of pH

The primary boundary in the adsorption cycle that affects metal particles and adsorbent surface charge may be the pH of the watery arrangement [27,28]. The tests were conducted at pH 3–14 because Pb (II), Cd (II) and Cr(IV) particles start to accelerate at pH 12 [29]. As found in figure 7c, expanding pH brings about expansion of adsorption limit from 68.55 to 108.58 mg/g. The justification for this outcome is that higher pH lead to more deprotonation of adsorbent surface that expands negatively charged locales, which is favoured for electrostatic fascination between surface of adsorbent and Pb (II) Cd(II) and Cr(IV) particles and consequently builds the adsorption limit. While, lower pH led to all the more decidedly charged destinations, which expands shock powers between adsorbent surface and Pb (II) Cd (II) and Cr (IV) particles that diminishes the adsorption limit [30]. Thus, pH 10-12 was considered for additional tests.

3.11 Adsorption thermodynamic

The thermodynamic studies revealed [illegible] in normal free energy change ΔG° (J/[illegible] ΔH° (J/mol) and entropy ΔS° (J/(molK)) were [illegible] by using three various thermodynamic ari[illegible]as mentioned [31].

$$K_D = q_e / C_e \quad ...(8)$$

$$\Delta G^0 = -RT \ln K_D \quad ...(9)$$

$$\ln K_D = (\Delta S^0 / R) - (\Delta H^0 / RT) \quad ...(10)$$

The findings demonstrate that as the temperature is raised from 25-50°C, the adsorption efficiency of Fe_3O_4/ZnO nanoparticles decreased from 109.1583-92.9709 (mg/g). This result suggests that the adsorption mechanism is thermodynamically favourable in exothermic reaction. The slope vs intercept can be used to match the values of ΔH° and ΔS° significantly. In addition, using equation 10, the ln G° value was K_D 1/T. Table 3 displays determined thermodynamic properties. A negative ΔH° indicates that the adsorption of Cd (II), Cr (IV) and Pb (II) onto Fe_3O_4/ZnO magnetic nanoparticles is exothermic in nature. A negative value for ΔS° denotes a reduction in the degree of freedom for adsorption species. Critical ΔG° also proves the component's feasibility and intentional electrostatic interactions. Similar results have been obtained for adsorption of Pb (II) by nano powder/alginate composite [32].

4. CONCLUSION

In this investigation, nanocomposites with a core-shell structure have been organized by using Fe_3O_4/ZnO nanocomposites presented in two stage approach and are used as an ideal alternative for lead, chromium and cadmium metal ion revocation from aqueous medium. This sorbent was characterized using various tools, like UV-vis[illegible], EDS, FTIR, VSM, FESEM, TEM and BET asse[illegible]dsorbent was rapid and stability was rea[illegible]pound 2 hr. The adsorption process can be e[illegible]ned by a pseudo-second-order kinetic model. The Langmuir isotherm model fit better with equilibrium data than Freundlich isotherm prototypes. Even so, maximum adsorption capability was 670.67 mg/g. ΔG°, ΔH° and ΔS° values were determined. Negative values of ΔG° and ΔH° indicate an attainable and exothermic adsorption mechanism, respectively. Such findings suggest that Fe_3O_4/ZnO nanocomposites might be used as an adsorbent for the elimination of Pb (II), Cr (IV), Cd (II) ions for commercial effluent.

ACKNOWLEDGEMENT

Authors would like to thank my research supervisor and extend thanks to our Department of Chemical Engineering, Annamalai University for providing facilities to carry out our work.

REFERENCES

1. Dhir, B. 2014. Potential of biological materials for removing heavy metals from wastewater. *Env. Sci. Poll.*, 21:1614-1627.
2. Abdel-Halim, S.H., A.M. Shehata and M.F. El-Shahat. 2003. Removal of lead ions from industrial wastewater by different types of natural materials. *Water Res.*, 37 (7): 1678-1683.
3. Barbosa, F. 2017. Toxicology of metals and metalloids: Promising issues for future studies in environmental health and toxicology. *J. Toxicol. Env. Health Part A*. 80(3):137–144.
4. Acharya, J., U. Kumar and B. Meikap. 2013. Thermodynamic characterization of adsorption of lead (II) ions on activated carbon developed from tamarind wood from aqueous solution. *South African J. Chem. Eng.*, 18 (1): 70-76.
5. Singha, B. and S.K. Das. 2012. Removal of Pb (II) ions from aqueous solution and industrial effluent using natural biosorbents. *Env. Sci. Poll. Res. Int.*, 19 (3): 2212-2226.
6. Hu, J., D. Zhao and X. Wang. 2011. Removal of Pb(II) and Cu(II) from aqueous solution using multi-walled carbon nanotubes/iron oxide magnetic composites. *Water Sci. Tech.*, 63(3): 917-923.
7. Dong, L., *et al.* 2010. Removal of lead from aqueous solution by hydroxyapatite/magnetite composite adsorbent. *Chem. Eng. J.*, 165: 827-834.
8. Kara, I., D. Yilmazer and S.T. Akar. 2017. Metakaolin based geopolymer as an effective adsorbent for adsorption of zinc(II) and nickel(II) ions from aqueous solutions. *Appl. Clay. Sci.*, 139(2): 54–63.
9. Qiu, R., F. Cheng and H. Huang. 2018. Removal of Cd from aqueous solution using hydrothermally modified circulating fluidized bed flyash resulting from coal gangue power plant. *J. Clean. Prod.*, 172(4):1918–1927.
10. Horst, M.F., M. Alvarez and V.L. Lassalle. 2016. Removal of heavy metals from wastewater using magnetic nanocomposites: Analysis of the experimental conditions. *Sep. Sci. Tech.*, 51(5): 550–563.
11. Hua, M. 2012. Heavy metal removal from water/wastewater by nanosized metal oxides: A review. *J. Hazard. Mater.*, 211(15):317–331.
12. Warner, C.L., *et al.* 2012. Manganese doping of magnetic iron oxide nanoparticles: Tailoring surface reactivity for a regenerable heavy metal sorbent. *Langmuir.* 28(8): 3931–3937.
13. Yan, J., *et al.* 2010. Facile coating of manganese oxide on tin oxide nanowires with high-performance capacitive behaviour. *ACS Nano*. 4(7): 4247- 4255.
14. Habibi, D., S. Kaamyabi and H. Hazarkhani. 2015. Fe_3O_4 nanoparticles as an efficient and reusable catalyst for the solvent-free synthesis of 99-dimethyl-9,10-dihydro-84-benzo-[a] xanthen-11(12H)-ones. *Chinese J. Catal.*, 36(3): 362-366.
15. Rajendran, S.P. and K. Sengodan. 2017. Synthesis and characterization of zinc oxide and iron oxide nanoparticles using *Sesbania grandiflora* leaf extract as reducing agent. *J. Nanosci.*, 17: 1-7.
16. Langmuir, I. 1916. The constitution and fundamental properties of solids and liquids. Part I. Solids. *J. American Chem. Soc.*, 38 (2):2221–2295.
17. Li, E., *et al.* 2016. Adsorption process of octadecyl amine hydrochloride on KCl crystal surface in various salt saturated solutions: Kinetics, isotherm model and thermodynamics properties. *J. Mol. Liq.*, 221(1): 949–953.
18. Fuku, X., A. Diallo and M. Maaza. 2016. Nanoscaled electrocatalytic optically modulated ZnO nanoparticles through green process of *Punica granatum* L. and their antibacterial activities. *Int. J. Electrochem.*, 124(2): 657-661.
19. Matinise, N., X.G. Fuku and K. Kaviyarasu. 2017. ZnO nanoparticles via *Moringa oleifera* green synthesis: Physical properties and mechanism of formation. *Appl. Surf. Sci.*, 406: 339–347.
20. Gupta, J.P., A. Hassan and K.C. Barick. 2021. Core-shell Fe_3O_4@ZnO nanoparticles for magnetic hyperthermia and bio-imaging applications. *AIP Adv.*, 11: 204-207.
21. Kumar, S.N., A. Zeenat and M.P. Kumar. 2020. Green synthesis of TiO_2 nanoparticles from *Syzygium cumini* extract for photocatalytic removal of lead (Pb) in explosive industrial wastewater. *Green Process Synth.*, 9(2): 171–181.
22. Saranya, K.S., *et al.* 2018. Green synthesis of high temperature stable anatase titanium dioxide nanoparticles using gum Kondagogu: Characterization and solar driven photocatalytic degradation of organic dye. *Nanomater. Base.*, 22(8): 1002-1021.
23. Xu, J., *et al.* 2006. Synthesis and optical properties of silver nanoparticles stabilized by gemini surfactant. *Colloid Surf. A.*, 273(4): 179 -183.
24. Kucharczyk, K., J.D. Rybka and M. Hilgendorff. 2019. Composite spheres made of bioengineered spider silk and iron oxide nanoparticles for theranostics applications. *PLoS ONE.* 14(7): 219 - 224.
25. Nassar, N. 2012. Kinetics equilibrium and thermodynamic studies on the adsorptive removal of nickel, cadmium and cobalt from wastewater by

superparamagnetic iron oxide nano adsorbents. *Canadian J. Chem. Eng.,* 90(3): 1231–1238.
26. Shayesteh, H., A. Rahbar-Kelishami and R. Norouzbeigi. 2016. Evaluation of natural and cationic surfactant modified pumice for Congo Red removal in batch mode: Kinetic, equilibrium and thermodynamic studies. *J. Mol. Liq.*, 221(4): 1-11.
27. Soltani, R. D., G.S. Khorramabad and G. Jorfi. 2014. Silica nano powders/alginate composite for adsorption of lead (II) ions in aqueous solutions. *J. Taiwan Inst. Chem. Eng.*, 45(2): 973–980.
28. Shu, Z. and S. Wang. 2009. Synthesis and characterization of magnetic nanosized / composite particles. *J. Nanometer.,* 1(5): 528-534.
29. Badruddoza, Z.M., *et al.* 2011. Carboxymethyl-a-cyclodextrin conjugated magnetic nanoparticles as nano adsorbents for removal of copper ions: Synthesis and adsorption studies. *J. Hazard. Mater.,* 185 (31): 1177–1186.
30. Nassar, N. 2010. Rapid removal and recovery of Pb (II) from wastewater by magnetic nano adsorbents. *J. Hazard. Mater.,* 184(3): 538–546.
31. Mehta, D., S. Mazumdar and K. Singh. 2015. Magnetic adsorbents for the treatment of wastewater - A review. *J. Water Process Eng.,* 7(3): 244–265.
32. Chen, J., *et al.* 2014. Novel core-shell structured Mn-Fe/ MnO_2 magnetic nanoparticles for enhanced Pb (II) removal from aqueous solution. *Ind. Eng. Chem. Res.,* 53(26): 10540-10548.